Enhancement of critical current densities by heavy-ion irradiation in $YBa_2Cu_3O_{7-\delta}$ observed using the high-resolution Faraday effect

Th. Schuster, H. Kuhn, M. R. Koblischka, H. Theuss, and H. Kronmüller
Max Planck Institut für Metallforschung, Institut für Physik, Heisenbergstrasse 1, D-7000 Stuttgart 80, Federal Republic of Germany

M. Leghissa, M. Kraus, and G. Saemann-Ischenko
Physikalisches Institut, Universität Erlangen, Erwin Rommel Strasse 1, D-8520 Erlangen, Federal Republic of Germany
(Received 24 August 1992)

Using the high-resolution Faraday technique, domain patterns of flux penetration in heavy-ion-irradiated $YBa_2Cu_3O_{7-\delta}$ thin films are obtained. To compare the influence of different projectiles, the samples were irradiated with 25-MeV oxygen ions, 230-MeV nickel ions, and 1-GeV lead ions with various fluences perpendicular to the sample surface and hence parallel to the c axis of the materials. The irradiation with ^{16}O produces point-defect cascades mainly perpendicular to the path of the projectile whereas the irradiation using ^{58}Ni ions creates spherical regions of amorphized material along the path. The ^{208}Pb ions create columnar tracks along the c axis of the material. For a simultaneous observation of irradiated and unirradiated regions of a single epitaxial thin film, only one-half of each sample was exposed to the irradiation. To obtain data for the acting-volume pinning forces and the local critical current densities, a numerical calculation also regarding the curvature of the flux lines is carried out. Oxygen and nickel irradiation lead to an enhancement of the critical current density by a factor of 2. By lead irradiation, an enhancement of the critical current density up to a factor of 5 is obtained. This critical current density at the largest fluence used reaches the theoretical predictions for an enhancement of the critical current density by means of irradiation-induced columnar tracks. The effects of the irradiation-induced defects are compared to those of the pinning sites present in the background pinning. The density of the irradiation-induced columnar defects and their influence on the pinning are compared to the density and effect of screw dislocations. Our results clearly indicate that screw dislocations do not act as effective pinning centers because of their small density.

I. INTRODUCTION

The high-energy heavy-ion irradiation provides a way to induce defects into superconductors that are well defined in number and shape. So, the influence of irradiation on the critical current density, j_c, and on the pinning potential was studied in many publications for the case of single crystals[1–7] and of sintered samples,[8–11] but only a few papers deal with irradiation influences on thin films. Roas *et al.*[12] studied the effect of 25-MeV oxygen irradiation in laser-ablated thin films. To date, only the experiments by Roas *et al.* and Schmitt[13] using 173-MeV Xe ions deal with the effect of columnar tracks on j_c in thin $YBa_2Cu_3O_{7-\delta}$ films.

Columnar tracks with a larger diameter are produced by 0.5-GeV iodine or 1-GeV lead irradiation. These defects have been shown in previous papers[2–7] to be the most effective pinning centers in single crystals. However, it is most interesting to study the influence of irradiation in samples which already show large critical current densities prior to irradiation.

Using the high-resolution Faraday (HRF) technique we are able to measure the acting pinning forces and critical current densities locally. This enables one to study the flux penetration simultaneously into irradiated and nonirradiated regions of a single sample under the same experimental conditions. This is the reason why of all our samples only a part of the sample was exposed to the irradiation. Previous magneto-optical experiments[4,6,7] have shown the advantages of the local observation studying the influence of irradiation-induced defects in high-T_c superconductors. Using a numerical calculation procedure it is possible to derive true values for the critical current densities from the Faraday observations in thin films.

The aim of this paper is to show domain patterns of the flux-line penetration in heavy-ion irradiated $YBa_2Cu_3O_{7-\delta}$ (YBCO) thin films and to compare the effects of irradiation on thin films and on single crystals to each other. The irradiation-induced defect density of columnar tracks produced by means of 1-GeV lead ions is compared to the density of screw dislocations in thin films which are described as an important pinning mechanism in previous papers.[14,15] In Sec. II, the sample preparation, characterization, and irradiation procedure will be presented. In Sec. III, the method used to calibrate the flux-density profiles and the numerical calculation of j_c also regarding the curvature of the flux lines is described. Section IV shows the results of the magneto-optical observations in partially irradiated thin films. In Sec. V, we will discuss the effects of different irradiations on the

critical current densities obtained and we compare the effect of irradiation-induced defects to the effect of screw dislocations and to the underlying background pinning. Finally, in Sec. VI we will summarize our results.

II. SAMPLE PREPARATION AND IRRADIATION

The experiments shown in this paper are carried out on two types of thin YBCO films. To allow a comparison with the earlier experiments of Roas *et al.*,[13] thin films prepared at Siemens Laboratories, Erlangen[16] are used. These films were prepared by laser ablation on $SrTiO_3$ substrates with a film thickness of 300 nm.

The other experiments were carried out on sputtered YBCO thin films.[17] These thin films were prepared by planar dc sputtering from a sintered, stoichiometric $YBa_2Cu_3O_{7-\delta}$ pellet. The temperature of the $SrTiO_3$ substrate was about 750 °C. For the chosen preparation conditions (O_2 pressure 2.3 mbar, distance target – substrate 19 mm) the deposition rate was 1.3 nm/min. The thickness of the film was measured by optical interference microscopy at an etched step to be 320 or 450 nm. The c-axis orientation was confirmed by x-ray diffraction. Typical T_c values for this preparation charge were about 87 K.

All samples were chemically patterned to a circular shape 2 mm in diameter. To obtain an easier handling in the various experimental stages, the samples were glued onto copper sample holders.

For all irradiations, the beam direction was chosen perpendicular to the surface of the thin films and hence parallel to the c axis of the materials. The oxygen irradiation was performed at the low-temperature facility of the tandem accelerator at the University of Erlangen. During the irradiation, the samples were cooled with liquid nitrogen and warmed up afterward to room temperature.

The irradiation with nickel ions was carried out at the Hahn-Meitner Institute, Berlin (VICKSI) at room temperature also with the beam direction perpendicular to the crystal surface. The irradiation with 1-GeV Pb ions was performed at GANIL (Caen, France) using the same arrangement of the samples and of the beam as at VICKSI. This irradiation was carried out at room temperature.

In order to study simultaneously the flux penetration in damaged and undamaged material we irradiated only one part of the sample while covering the other part with an absorber. Effects of ion implantation could safely be neglected due to the small thickness of the thin films compared to the projected range of the projectiles (approximately 20 μm).[4] The irradiation fluences are chosen to allow a comparison with the previous papers by Roas *et al.*[12] (irradiation with 25-MeV oxygen ions) and with results on single crystals.[4,6,7]

For use with the HRF technique, all samples were carefully cleaned before the coating with the Al layer ($\approx$ 100-nm thick) and with the magneto-optical active coating of EuSe ($\approx$ 200-nm thick).

III. FARADAY EFFECT

The experiments are performed using the optical cryostat and microscope which is described in detail in Refs. 18 and 19. Observations by means of the HRF technique are possible only in the temperature range 5 K $\leq T \leq$ 20 K. The lower temperature limit is given by the technology of the cryostat, the upper boundary is imposed by the temperature-dependent Verdet constant of the europium chalcogenides.[20] In this paper we show observations of the Shubnikov phase at a temperature of $T = 5$ K. The images can be observed directly at the microscope or may be transferred to an image-processing system for analyzing purposes.[21] The external magnetic field is generated by a copper solenoid coil producing a maximum field of 0.3 T. However, the method to obtain the critical current densities is different from the paper dealing only with single crystals.[6,20] First, the calibration technique shown in Ref. 22 is followed. To calibrate the measured intensity, I, in terms of the local flux density, B_z, two fixed points are determined: In the Meissner phase at the center of the sample we have $B_z = 0$ mT. Far away from the sample edge on the $SrTiO_3$ substrate, the measured intensity corresponds directly to the external field, $\mu_0 H_{\text{ext}}$. Using these fixed points, every intensity measured can be expressed in terms of B_z.

The critical current density can be expressed as

$$\mathbf{j}_c = (1/\mu_0) \cdot \text{curl}\mathbf{B}. \tag{1}$$

In the case of a circular sample showing a radially symmetric penetration of the flux follows (in cylindrical coordinates):

$$j_{c,\Phi} = 1/\mu_0 \left[\frac{\partial B_z}{\partial r} - \frac{\partial B_r}{\partial z} \right] \tag{2}$$

and

$$f_{p,r} = j_c B_z. \tag{3}$$

As shown in Ref. 23, the critical current density is governed not only by the usual flux-density gradient $\partial B_z/\partial r$ but also by the gradient

$$\left| \frac{\partial B_r}{\partial z} \right| \approx \left| \frac{\partial B_z}{\partial r} \right| \frac{R}{d} \tag{4}$$

which is larger by the factor R/d. The relation (4) holds for films with a thickness, d, lower than the London penetration depth, λ_L, as long as the applied field is below the full penetration field, $\mu_0 H^*$. In the case of a thin film with a thickness $d = 500$ nm and a radius $R = 1$ mm the factor R/d is approximately 2000. As the HRF technique allows only a detection of $\partial B_z/\partial r$, a numerical calculation technique was developed in Ref. 24, based on previous calculations.[25–27] For these calculations, the current distribution, $j(r)$, in the film is approximated by N concentric current loops which are spaced equidistantly so that the measurement is reproduced via the Biot-Savart law. This model corresponds to a homogeneous current density distribution in the z direction. Such an approximation is valid for films with a thickness d lower than

the London penetration depth, λ_L. To obtain the gradient $\partial B_r/\partial z$, a numerical fit to the data is performed (see Fig. 2). From this fit, not only this gradient could be calculated but also the resulting critical current density, j_c.

IV. MAGNETO-OPTICAL OBSERVATIONS

All magneto-optical observations presented throughout this paper are carried out at a temperature $T = 5$ K. The external magnetic field is in all cases applied perpendicular to the sample surface and therefore parallel to the c axis of the material. The Shubnikov phase is imaged as bright domains, the Meissner phase remains dark. In all images presenting domain structures, the left half of the all thin films is the irradiated region whereas the right half is unirradiated.

A. Oxygen irradiation

To allow a comparison to the earlier experiments by Roas *et al.*,[8] samples prepared at Siemens Laboratories, Erlangen, with a thickness $d = 300$ nm are used for the observations. The irradiation fluences chosen for our experiments are in the range where an enhancement of the critical current density, j_c, was found in the previous work of Roas *et al.*[8]

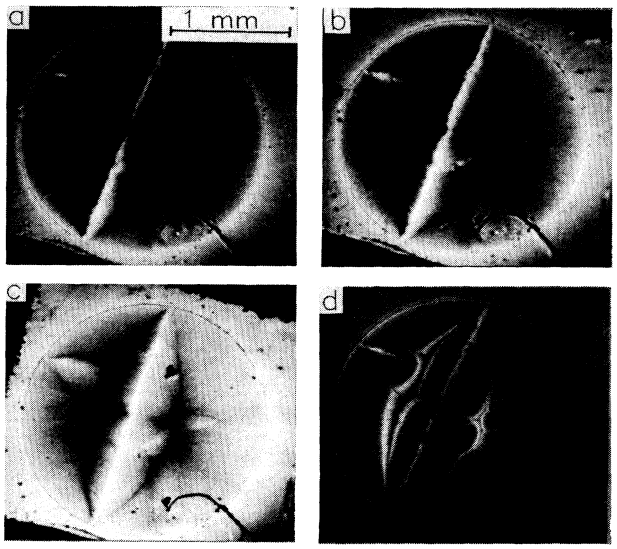

FIG. 1. Domain patterns observed on sample Y4 (oxygen irradiation, $\Phi t = 6.0 \times 10^{14}$ ions/cm^2). The Shubnikov phase is imaged as bright domains, the Meissner phase remains dark. On the substrate, which is also covered with the magneto-optical active layer, the local flux density, B_z, outside of the sample is detected. Only the left half of the sample was exposed to the irradiation. (a) $\mu_0 H_{\rm ext} = 27$ mT. Due to the large demagnetizing factor of the thin film, the flux penetrates immediately along the border between the irradiated and the nonirradiated parts of the sample. (b) $\mu_0 H_{\rm ext} = 109$ mT. (c) $\mu_0 H_{\rm ext} = 273$ mT. The full penetration field, $\mu_0 H^*$, is nearly reached in the nonirradiated area. (d) The corresponding remanent state ($\mu_0 H_{\rm ext} = 0$ mT) to (c). At the sample edges, flux lines of negative sign are clearly visible.

As an example for our experimental procedure on thin films, we show domain patterns of an oxygen-irradiated sample (Y4, irradiated at a fluence $\Phi t = 6.0 \times 10^{14}$ ions/cm^2). In Figs. 1(a)–1(d), the domain structures of sample Y4 are presented. Only the left half of the sample was exposed to the irradiation. High-quality thin films which are patterned as circles show a radial flux penetration. This was already pointed out in Refs. 17 and 22. If the critical current density is markedly changed in the irradiated half of the sample as is the case in the sample presented here, the flux penetration is different as a deeper flux penetration is found in the nonirradiated area. The radial symmetric flux penetration is additionally disturbed at the border between the irradiated and nonirradiated regions of the sample which is due to the differences in the critical current densities flowing along the gradients toward the Meissner regions. Due to the large demagnetizing factors of the thin film samples, this behavior is clearly visible and much stronger as compared to the behavior of the single crystals. As pointed out already in Ref. 7, the domain pattern of a partly irradiated sample enables one to reconstruct the domain structures which would be obtained in an unirradiated or a fully irradiated sample if the sample is defect-free and regularly patterned. An important feature for thin films is clearly visible in the figure as the local flux density, B_z, shows a large enhancement at the sample edge. This behavior is also shown in the flux-density profiles of Fig. 2.

Figure 1(a) shows the domain structure obtained at $\mu_0 H_{\rm ext} = 27$ mT. It is clearly visible that the two parts of the sample act independently from each other. In Fig. 1(b) ($\mu_0 H_{\rm ext} = 109$ mT), the flux begins to penetrate into the irradiated region starting from the border between the irradiated and the nonirradiated region. Figure 1(c) shows the sample at an external field $\mu_0 H_{\rm ext} = 273$ mT. The full-penetration field, $\mu_0 H^*$, is nearly reached in the unirradiated area whereas in the irradiated area a small Meissner phase resides indicating an enhancement of the critical current density, j_c. As shown also in Table I, j_c is enhanced by a factor of 2. Figure 1(d) presents the remanent state after applying an external magnetic field of $\mu_0 H_{\rm ext} = 273$ mT. As shown in previous papers,[17,28,29] a remanent state in a high-T_c sample consists of three domains: Beginning at the sample edge, newly entered flux lines of negative sign are found. This bright domain is followed by the so-called annihilation zone ($B_z = 0$, dark belt) separating the domain of pinned vortices (also imaged as a bright domain). For the pinned vortices we use the term "positive direction" whereas the newly entered vortices are called "negative" or inverse vortices. The annihilation zone is due to an attractive interaction between the vortices of different sign leading to an annihilation of flux lines. The negative flux lines are caused by the stray fields of the pinned vortices. In the unirradiated area of the crystal, the domain of inverse vortices is much larger showing the coupled behavior between the two kinds of vortices.

Flux-density profiles measured in irradiated and unir-

TABLE I. Critical current densities obtained for oxygen-irradiated (25-MeV) YBCO thin films. These samples were prepared at Siemens Laboratories, Erlangen, using laser-ablation technique. The film thickness is 300 nm. $j_c(0)$ denotes the critical current density of the unirradiated area, $j_c(\Phi t)$ the critical current densities obtained after irradiation. The temperature in the experiments is $T = 5$ K.

Sample	Φt (10^{14} ions/cm^2)	$j_c(0)$ (10^7 Å/cm^2)	$j_c(\Phi t)$ (10^7 Å/cm^2)	$j_c(\Phi t)/j_c(0)$
Y1	1.0	3.6	3.6	1.0
Y2	2.0	3.2	3.8	1.2
Y3	4.0	4.5	5.7	1.3
Y4	6.0	4.0	7.2	1.9

radiated areas of the sample as presented above are shown in Fig. 2. The upper plot corresponds to the nonirradiated area, the lower plot to the irradiated region. The symbols denote the measured data, the solid lines the corresponding numerical fits. Corresponding to the semiempirical method introduced in Ref. 24, a current density distribution, $j(r)$, can be fitted to the experimental data, $B_z(r)$, so that the measurement is reproduced via the Biot-Savart law. From this current density distribution, the radial field component, $B_r(r)$, which is at the moment not accessible to the experiment, can be calculated (see Fig. 3). The center of the sample is located at $r = 0$, the sample edge at $r = 1$. For the flux-density profiles shown, the flux penetration starting from the border is neglected. As in such partly irradiated samples the radial symmetry of flux penetration into the whole sample is disturbed, the flux-density profiles are read in homogeneous regions showing a radial penetration of flux. For the calibration in terms of the flux density, B_z, it is necessary to read also data outside of the sample, e.g., the local flux density on the substrate.[22] The flux-density profiles into the samples are nearly linear in this field range and show a large overshoot at the sample edge. This overshoot reflects the large demagnetizing factors of the thin films. The flux-density profiles of the irradiated region show this behavior as more expressive as the profile obtained at $\mu_0 H_{\text{ext}} = 41$ mT has a maximum at $B_z = 109$ mT. In the unirradiated area, the profile measured at $\mu_0 H_{\text{ext}} = 55$ mT has an overshoot up to $B_z = 110$ mT.

The numerically fitted flux-density profiles allow a calculation of the undetectable gradient, $\partial B_r/\partial z$. The results of this numerical calculation are shown in Fig. 3

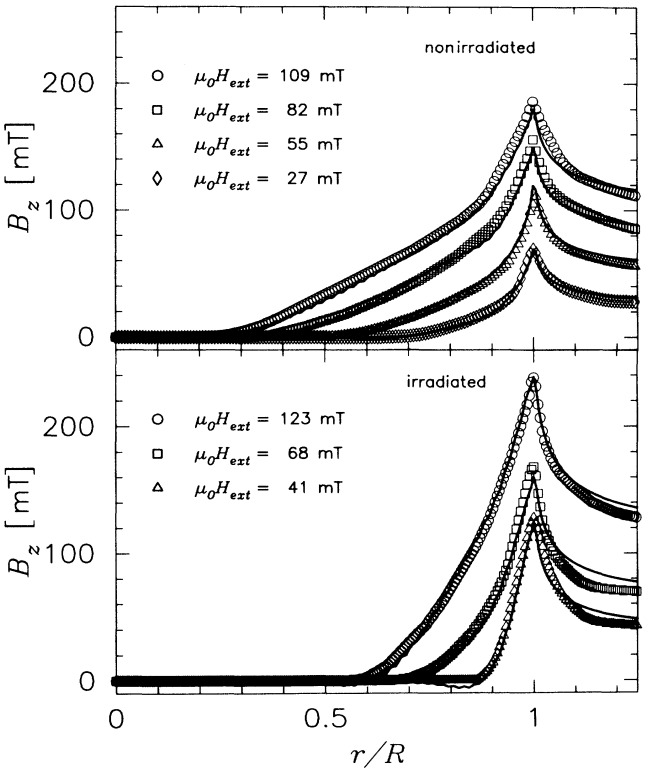

FIG. 2. Flux-density profiles obtained at sample Y4 at various external magnetic fields. The upper plot illustrates the measured profiles in the nonirradiated area, the lower plot shows the flux-density profiles of the irradiated region. The flux-density profiles are read radially; the point $r = 0$ denotes the center of the sample, $r = 1$ the sample edge. The symbols are the measured data, the solid lines denote the numerical fits to the data.

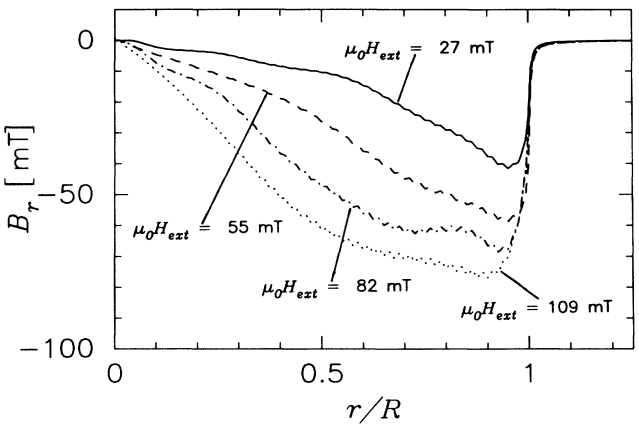

FIG. 3. Numerical calculations of the undetectable flux gradient, $\frac{\partial B_r}{\partial r}$ using the model described in Ref. 15. The data shown correspond directly to the flux-density profiles $B_z(r)$ of the nonirradiated area of the thin film (upper plot of Fig. 2).

at various applied external fields for the unirradiated region. B_r denotes the radial component of the magnetic induction [see also Eq. (2)]. It is clearly visible that B_r is largest at the sample edge. To the center of the sample, B_r shows a large, monotonous decrease.

In Fig. 4, the behavior of the volume pinning force, f_p, on the local flux density, B_z, is shown for both regions. In this low-field regime, the volume pinning forces are continuously growing. Clearly visible is the enhancement of f_p due to the irradiation (see also the j_c data given in Table I). Sample Y4 shows an enhancement of the critical current density by a factor of 1.9.

Fluence-dependent observations of all samples Y1–Y4 are shown in Figs. 5(a)–5(h) at the same external fields $\mu_0 H_{\rm ext} = 27$ and 109 mT. In Figs. 5(a) and 5(b), sample Y1 is shown ($\Phi t = 1.0 \times 10^{14}$ ions/cm^2). As is also visible from Table I, no differences between the irradiated and unirradiated regions is found. Sample Y2 [Figs. 5(c) and 5(d)], irradiated at $\Phi t = 2.0 \times 10^{14}$ ions/cm^2, is represented. Due to the large demagnetizing effects occurring at surface irregularities these regions are immediately penetrated by the flux. A small difference between the two regions can be detected. In sample Y3, irradiated at $\Phi t = 4.0 \times 10^{14}$ ions/cm^2 [Figs. 5(e) and 5(f)], this behavior becomes more obvious. Also, the differences between the penetration depths in both areas are well visible. Figures 5(g) and 5(h) present again the sample Y4 ($\Phi t = 6.0 \times 10^{14}$ ions/cm^2) for comparison with the other samples.

The data for the critical current densities $j_c(0)$, which are measured in the nonirradiated region, and $j_c(\Phi t)$ obtained from irradiated areas are summarized in Table I. The data for the critical current density are nearly constant in the field range 0 – 0.15 T. To allow a comparison of data measured on various thin films, also the relative enhancement, $j_c(\Phi t)/j_c(0)$, is listed in the Table. In this way, the data become comparable with each other in spite of the scatter of the sample quality. Sample Y1 shows no enhancement of the critical current density due to the irradiation. In samples Y2 – Y4, a continuous growing of the relative enhancement of the currents is found.

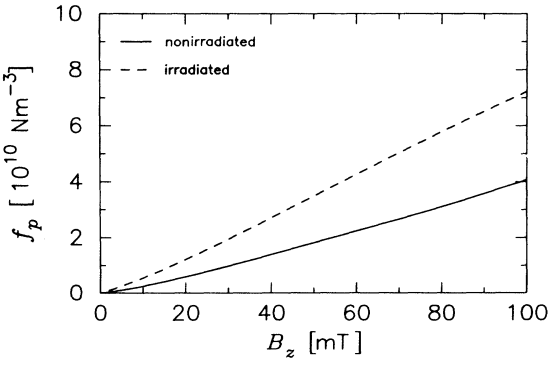

FIG. 4. Dependence of the calculated local volume pinning force density, f_p, on the local field, B_z, of the sample Y4. The solid line corresponds to the nonirradiated area, the dashed line denotes the data after irradiation. In this field regime, the $f_p(B_z)$ curves are stetic growing.

B. Nickel irradiation

For this kind of irradiation, sputtered thin films (University of Erlangen) with a thickness of $d = 450$ nm are

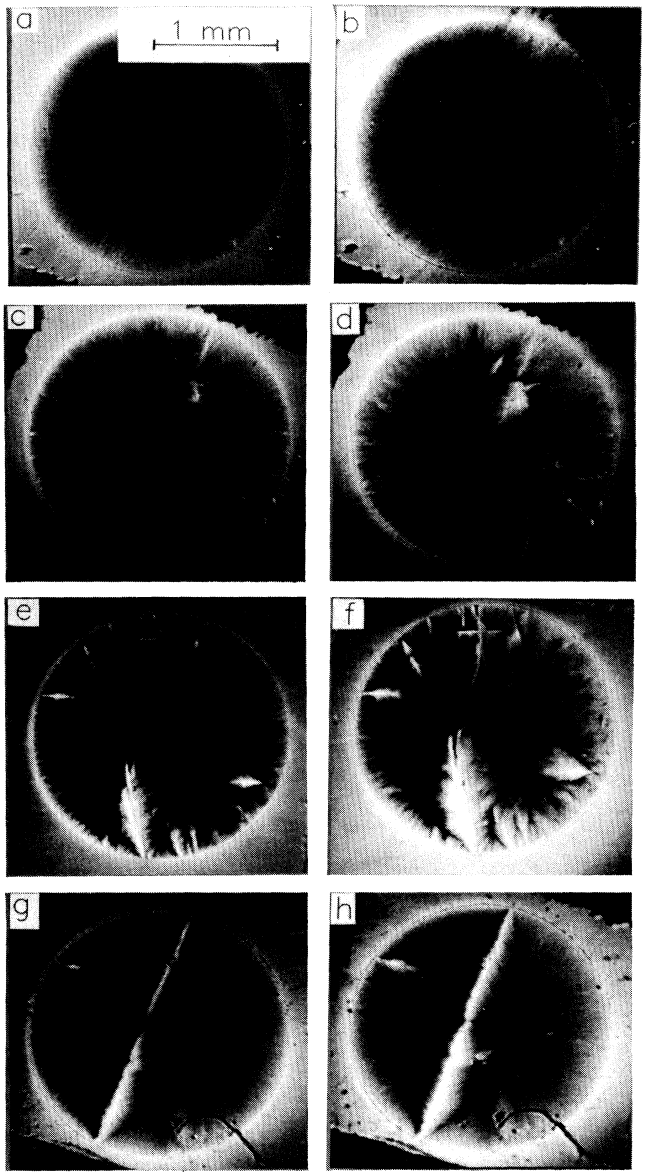

FIG. 5. Fluence dependence of the domain patterns obtained from oxygen irradiated samples. All thin films (laser-ablated films prepared at Siemens Laboratories, Erlangen) have the same thickness of 300 nm. (a) Sample Y1, irradiated at $\Phi t = 1.0 \times 10^{14}$ ions/cm^2. The external magnetic field is $\mu_0 H_{\rm ext} = 27$ mT. (b) $\mu_0 H_{\rm ext} = 109$ mT. No visible difference between the two areas is found in this sample. (c) Sample Y2, irradiated at $\Phi t = 2.0 \times 10^{14}$ ions/cm^2. The external magnetic field is $\mu_0 H_{\rm ext} = 27$ mT. (d) $\mu_0 H_{\rm ext} = 109$ mT. (e) Sample Y3, irradiated at $\Phi t = 4.0 \times 10^{14}$ ions/cm^2. The external magnetic field is $\mu_0 H_{\rm ext} = 27$ mT. (f) $\mu_0 H_{\rm ext} = 109$ mT. (g) Sample Y4, irradiated at $\Phi t = 6.0 \times 10^{14}$ ions/cm^2. The external magnetic field is $\mu_0 H_{\rm ext} = 27$ mT. (h) $\mu_0 H_{\rm ext} = 109$ mT.

TABLE II. Critical current densities obtained for nickel-irradiated YBCO thin films. These experiments are carried out on sputtered thin films with a film thickness of 450 nm. $j_c(0)$ denotes the critical current density of the unirradiated area, $j_c(\Phi t)$ the critical current densities obtained after irradiation. The temperature in the experiments is $T = 5$ K.

Sample	Φt (10^{11} ions/cm^2)	$j_c(0)$ (10^7 Å/cm^2)	$j_c(\Phi t)$ (10^7 Å/cm^2)	$j_c(\Phi t)/j_c(0)$
Y5	2.0	5.0	6.0	1.2
Y6	5.0	3.8	5.2	1.4
Y7	10.0	3.6	6.9	1.9

used. The fluences of irradiation are chosen so as to obtain an enhancement of j_c at every fluence. In Figs. 6(a)–6(f), dose-dependent measurements on 230-MeV nickel-irradiated samples are presented. For each sample Y5–Y7 two external applied magnetic fields ($\mu_0 H_{ext} = 68$ and 178 mT) are shown. Also in this case, the flux penetrates the sample radially. Figures 6(a) and 6(b) show sample Y5 ($\Phi t = 2.0 \times 10^{11}$ ions/cm^2). The differences found in the irradiated and nonirradiated regions are relatively small. Figures 6(c) and 6(d) present sample Y6, irradiated at $\Phi t = 5.0 \times 10^{11}$ ions/cm^2. The influence of irradiation becomes more intensive as compared to sample Y5. Sample Y7 [Figs. 6(e) and 6(f)], irradiated at ($\Phi t = 1.0 \times 10^{12}$ ions/cm^2), illustrates clearly the influence of irradiation as in the unirradiated region the full penetration field, $\mu_0 H^*$, is nearly reached at $\mu_0 H_{ext} = 178$ mT, whereas in the irradiated area a large amount of Meissner phase is present in the sample. The results for the critical current densities, $j_c(0)$ and $j_c(\Phi t)$, are summarized in Table II. All samples show an enhancement of the critical current density due to irradiation, but the results are similar to the oxygen irradiation as nearly the same maximum enhancement is obtained. The fluences chosen for these experiments are identical to the DyBCO single crystals presented in Ref. 7, so the results can be compared directly.

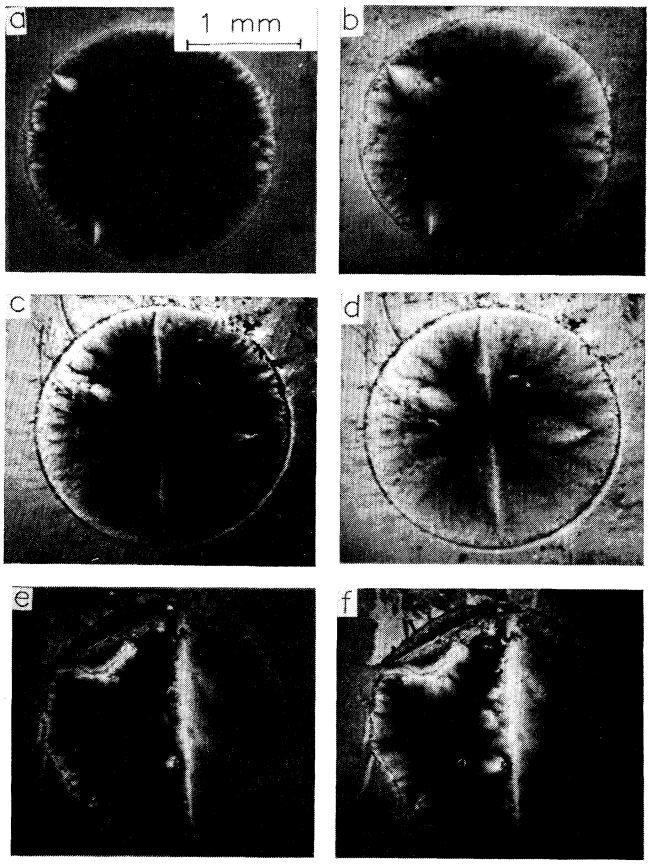

FIG. 6. Fluence dependence of the domain patterns after 230-MeV Nickel irradiation. The YBCO thin films were prepared at the University of Erlangen using a sputter technique; the film thickness is 450 nm. (a) Sample Y5, $\Phi t = 2.0 \times 10^{11}$ ions/cm^2, $\mu_0 H_{ext} = 68$ mT. (b) $\mu_0 H_{ext} = 178$ mT. (c) Sample Y6, $\Phi t = 5.0 \times 10^{11}$ ions/cm^2, $\mu_0 H_{ext} = 68$ mT. (d) $\mu_0 H_{ext} = 178$ mT. (e) Sample Y7, $\Phi t = 1.0 \times 10^{12}$ ions/cm^2, $\mu_0 H_{ext} = 68$ mT. (f) $\mu_0 H_{ext} = 178$ mT. This sample is the only one of this series showing a visible irradiation effect.

C. Lead irradiation

As pointed out in Refs. 3 and 7, the lead irradiation produces columnar defects along the c axis of the films using the arrangement of beam and sample as in this paper. Accordingly, this kind of irradiation is expected to create the most effective pinning centers. Also, for this kind of irradiation the sputtered YBCO thin films with a thickness $d = 450$ nm are used.

Figures 7(a)–7(h) present domain patterns of samples Y8–Y11 irradiated at different fluences. The external applied magnetic fields are the same for each series, e.g., $\mu_0 H_{ext} = 27$ and 109 mT except for sample Y10. Figures 7(a) and 7(b) show sample Y8 which was irradiated at $\Phi t = 7.0 \times 10^{10}$ ions/cm^2. No visible difference between the irradiated and the unirradiated half can be found in the domain patterns. The same behavior is obtained on sample Y9 [Figs. 7(c) and 7(d); $\Phi t = 9.0 \times 10^{10}$ ions/cm^2]. Then, Figs. 7(e) and 7(f) illustrate the domain patterns obtained on sample Y10, which was irradiated at $\Phi t = 10.0 \times 10^{10}$ ions/cm^2. In this sample, a slight difference in the flux penetration is found (see also Table III). Note that the external magnetic fields are different from the rest of the series ($\mu_0 H_{ext} = 14$ and 34 mT), as the sample has a smaller thickness $d = 320$ nm. This smaller thickness leads to an even larger demagnetizing factor, so the flux penetrates deeper into the sample at the same external magnetic fields. In Figs. 7(g) and

7(h), sample Y11 irradiated at $\Phi t = 30.0 \times 10^{10}$ ions/cm^2 is shown. This sample presents a large enhancement of j_c from 1.3×10^7 Å/cm^2 to 6.7×10^7 Å/cm^2 yielding a factor of enhancement of 5.1. The data obtained for this sample reach the theoretical limit as calculated in Refs. 6 and 28. This will be discussed in Sec. V. The domain pattern [Fig. 7(h)] shows a large Meissner phase in the irradiated region whereas in the unirradiated area of the sample, the full penetration field, $\mu_0 H^*$, is reached already.

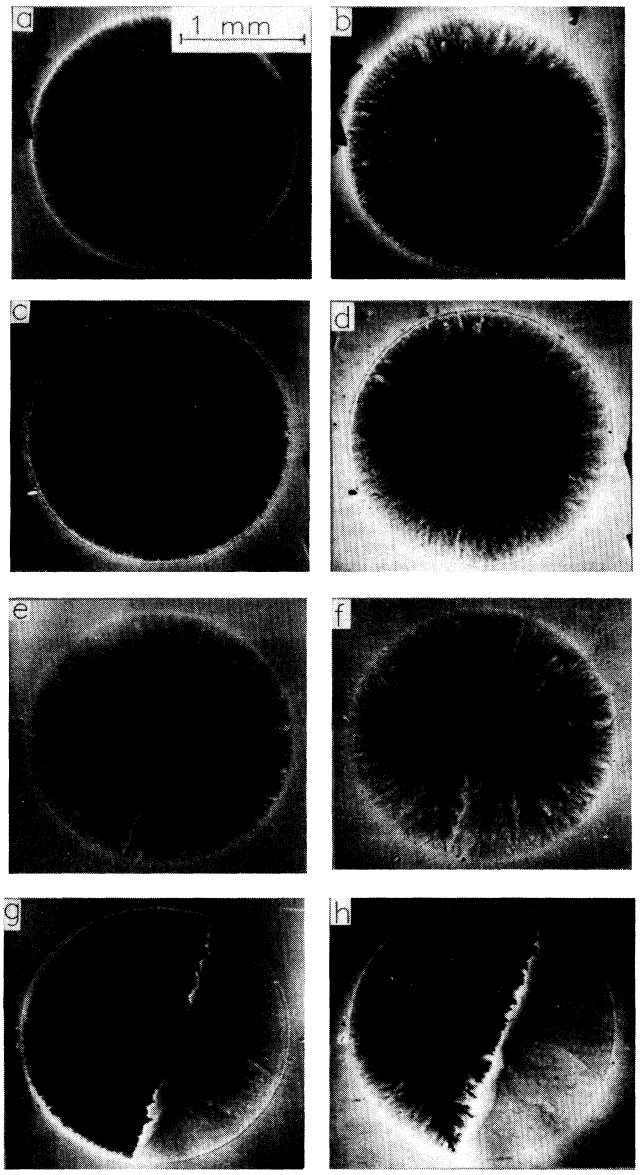

FIG. 7. Fluence dependence of the domain patterns after lead irradiation (1-GeV lead ions). These experiments are also performed on sputtered YBCO thin films with a thickness of 450 nm. (a) Sample Y8, irradiated at $\Phi t = 7.0 \times 10^{10}$ ions/cm^2, $\mu_0 H_{\text{ext}} = 27$ mT. (b) $\mu_0 H_{\text{ext}} = 109$ mT. The domain pattern shows no visible difference between irradiated and unirradiated areas. (c) Sample Y9 ($\Phi t = 9.0 \times 10^{10}$ ions/cm^2), $\mu_0 H_{\text{ext}} = 27$ mT. (d) $\mu_0 H_{\text{ext}} = 109$ mT. Also this sample shows a radial symmetric flux penetration. (e) Sample Y10 ($\Phi t = 10.0 \times 10^{10}$ ions/cm^2), $\mu_0 H_{\text{ext}} = 14$ mT. (f) $\mu_0 H_{\text{ext}} = 35$ mT. (g) Sample Y11, irradiated at $\Phi t = 30.0 \times 10^{10}$ ions/cm^2, $\mu_0 H_{\text{ext}} = 27$ mT. This sample is the only one in this series showing a large enhancement of j_c. (h) $\mu_0 H_{\text{ext}} = 109$ mT.

In Table III, the data for the critical current densities are summarized. Samples Y8 and Y9 show no enhancement of j_c due to irradiation. In sample Y10, only a small enhancement is detected, whereas sample Y11 shows a large enhancement of $j_c(\Phi t)$ as expected from the results on single crystals.[1]

V. DISCUSSION

The high-resolution Faraday effect (HRF) technique provides a useful tool to study the effect of irradiation also in thin films of high-T_c superconductors. The results presented in Sec. IV show the advantages of the local observations of Shubnikov phase which are possible using the HRF technique. This allows a simultaneous observation of flux penetration in irradiated and unirradiated parts of one sample. By this method, experiments before and after irradiation, which are unavoidable in other experiments due to a scatter in sample quality, can be avoided by using the HRF technique.

As already mentioned in the discussion to Fig. 1, it is possible to reconstruct the domain structure which would be obtained on a nonirradiated or fully irradiated thin film starting from the domain pattern of a partly irradiated, defect-free sample which is regularly patterned.

The irradiations with 0.5-GeV iodine ions and 1-GeV Pb ions produce columnar tracks along the projectile paths in the target materials.[2–7] Magneto-optical observations on iodine-irradiated single crystals are shown in Refs. 4, 6, and 7. Such defects act as effective pinning centers if the external field is oriented parallel to the tracks. Our results also allow us to compare the different influences of 25-MeV oxygen irradiation, 230-MeV nickel irradiation, and 1-GeV lead irradiation on the pinning behavior.

So, it is most interesting to study the effect of lead irradiation which proved to create the most effective pinning centers,[7] also in thin YBCO films which already show large critical current densities prior to irradiation. From the results obtained in Refs. 1–7, a large enhancement of the critical current densities was expected also in the YBCO thin films. However, as it can be seen from Table III, on the samples irradiated at low fluences (sample Y8: $\Phi t = 7.0 \times 10^{10}$ ions/cm^2, sample Y9: $\Phi t = 9.0 \times 10^{10}$ ions/cm^2) no differences in the radial flux penetration into irradiated and nonirradiated areas are found thus leading to no enhancement of the critical current density. Only the sample irradiated at $\Phi t = 30.0 \times 10^{10}$ ions/cm^2 (sample Y11) shows an enhancement of j_c. What is the reason for such a behavior?

To find an explanation we consider at first the results on lead-irradiated single crystals to allow a direct comparison with the results obtained in this paper. On lead-irradiated Bi 2:2:1:2 and DyBCO single crystals,[7]

TABLE III. Critical current densities obtained for lead-irradiated YBCO thin films. For these experiments, sputtered thin films with a thickness of 450 nm are used. $j_c(0)$ denotes the critical current density of the unirradiated area, $j_c(\Phi t)$ the critical current densities obtained after irradiation. The temperature of the experiment is $T = 5$ K.

Sample	Φt (10^{10} ions/cm^2)	$j_c(0)$ (10^7 Å/cm^2)	$j_c(\Phi t)$ (10^7 Å/cm^2)	$j_c(\Phi t)/j_c(0)$
Y8	7.0	6.8	6.8	1.0
Y9	9.0	3.8	3.8	1.0
Y10	10.0	1.3	1.4	1.1
Y11	30.0	1.3	6.7	5.1

an enhancement from $j_c(0) = 3.3 \times 10^5$ Å/cm^2 to 30.5×10^5 Å/cm^2 was obtained for Bi 2:2:1:2 crystals and from $j_c(0) = 2.1 \times 10^5$ Å/cm^2 to 40.5×10^5 Å/cm^2 for DyBCO crystals also using 1-GeV lead ions with a fluence $\Phi t = 9.0 \times 10^{10}$ ions/cm^2 (Bi 2:2:1:2) and a fluence $\Phi t = 10.0 \times 10^{10}$ ions/cm^2 (DyBCO). These data reveal that a limit for the attainable critical current density exists for every fluence and every projectile which does not depend on the target material. This behavior was found in Ref. 7 investigating two types of single crystals and different kinds of irradiation (lead ions, iodine ions). Based on calculations by Conner and Malozemoff,[27] we may assume that the critical current density of single crystals determined by using the HRF technique is about a factor 2–3 too low since the effect of flux-line curvature was not considered. So, a limit for the critical current density, $j_{c,\mathrm{lim}} = 1.2 \times 10^7$ Å/cm^2 at a fluence $\Phi t = 10.0 \times 10^{10}$ ions/cm^2 results.

In previous papers[2,6,30] the maximum attainable critical current density, $j_{c,\mathrm{max}}$, due to irradiation-induced columnar tracks was calculated to $j_{c,\mathrm{max}} = 6$–7×10^7 Å/cm^2, regarding the interaction of one single vortex with one columnar track. The difference between the calculated value, $j_{c,\mathrm{max}}$, and the measured limit, $j_{c,\mathrm{lim}}$, on single crystals at smaller irradiation fluences than $< 30.0 \times 10^{10}$ ions/cm^2 can be explained by taking into account the local distribution of the irradiation-induced columnar tracks in the sample.[2,31] If the columnar tracks are equally distributed, we are able to calculate a dose-equivalent field, B_Φ, where the number of flux lines in the sample equals the number of defects. This field can be expressed as $B_\Phi = \Phi_0 \cdot (\Phi t)$, with Φ_0 denoting the elementary flux quantum. At a fluence $\Phi t = 10.0 \times 10^{10}$ ions/cm^2, a dose-equivalence field of 2 T results which is considerably larger than our field range 0–0.3 T. As in reality the defect density varies locally, pinning-free paths for the flux lines result. So, not all flux lines are pinned at the columnar tracks thus leading to a smaller critical current density as calculated with $j_{c,\mathrm{max}}$.

Table III shows that the critical current densities of the unirradiated thin films [$j_c(0)$ of samples Y8 and Y9] are larger than the limit, $j_{c,\mathrm{lim}}$, due to irradiation-induced columnar tracks obtained on single crystals. For sample Y10 we obtained $j_c(0) = 1.3 \times 10^7$ Å/cm^2; this value corresponds to $j_{c,\mathrm{lim}}$. In this sample, an irradiation-induced enhancement of j_c up to $j_c(\Phi t) = 1.4 \times 10^7$ Å/cm^2 is found. In sample Y11, irradiated at a fluence $\Phi t = 30.0 \times 10^{10}$ ions/cm^2, an enhancement of j_c by a factor of 5.1 up to $j_c(\Phi t) = 6.7 \times 10^7$ Å/cm^2 is obtained; this value corresponds to the theoretical limit, $j_{c,\mathrm{max}}$. As already found in the investigations on lead-irradiated single crystals, at this fluence a maximum enhancement of j_c is obtained because, due to the matching effect, all vortices are pinned at irradiation-induced defects. So, a further increase of the irradiation fluence is expected to yield no further enhancement of the critical current density in the field range investigated here. If the sample Y8, showing already a $j_c(0) = 6.8 \times 10^7$ Å/cm^2 prior to irradiation, would be irradiated with our largest fluence, we expect that no enhancement of the critical current density would be observed. As shown in the flux-density profiles of Figs. 2 and 3, another important point is given by the curvature of the flux lines in the thin film samples. The columnar tracks induced by lead irradiation are oriented parallel to the c axis of the superconductors and, therefore, are straight defects. The curvature of the flux lines implies that a vortex could not be pinned on the whole length by such a straight defect. Following the description given in Ref. 32, the maximum tilt angle, α_{max}, can be written as

$$\alpha_{\mathrm{max}} = \tan^{-1}(Jd/2H). \tag{5}$$

In this equation, J denotes the current density, d the thickness of the sample, and H the external magnetic field. Equation (5) is valid for large demagnetizing factors, e.g., if $d \ll R$ (R denotes the sample radius). For a current density of 2.0×10^7 Å/cm^2 and a thickness $d = 450$ nm, a maximum tilt angle between 65° and 15° results in the field range of 10–150 mT used in our observations. In reality, the resulting tilt angles are smaller because in Eq. (5) the influence of the line tension and of the pinning are not considered. Table III shows that in sample Y11 a large enhancement of j_c is obtained. At a large fluence like $\Phi t = 30.0 \times 10^{10}$ ions/cm^2 a large density of defects results. As measured in TEM investigations,[2] the diameter of the columnar tracks is approximately 10 nm. If we calculate the resulting density of defects induced at this fluence, 23% of the sample should be covered with such defects. With such a density of defects, a curved flux line intersects many columnar tracks due to the small distance between the defects. At a tilt angle of 45 ° ($\mu_0 H = 50$ mT) and with the data given above, a curved flux line intersects about 5–6 latent

tracks, if we assume the tracks to be spaced equidistantly. In Figs. 7(g) and 7(h) the overshoot of the local flux density, B_z, is clearly visible in both regions of the sample indicating the large demagnetizing factor and the presence of curved flux lines. As a concluding remark we note that even if the tilt angles calculated using Eq. (5) are present in the sample the columnar tracks will still act as an effective pinning center as a curved flux line intersects many such defects at high defect densities. If the flux lines are not strongly curved the straight columnar tracks act as well as very effective pinning sites as found in the investigations on single crystals. The irradiation using 230-MeV nickel ions creates spherical regions of amorphized material like "pearl chains" of defects along the projectile path. The diameter of the so-produced channels is smaller than that of the columnar tracks created by iodine or lead irradiation. So the condition for the calculation of $j_{c,\max}$ on the basis of linear defects is not fulfilled in this case. If we compare the results of the Ni irradiation on the DyBCO single crystals of the previous paper[7] to the data obtained on samples Y5–Y7, the relative enhancement of j_c is approximately the same. This clearly shows the influence of irradiation regardless of the type of the defect structure. However, the effective values for $j_c(0)$ and $j_c(\Phi t)$ are larger for thin films. The sample Y7, irradiated at a fluence $\Phi t = 1.0 \times 10^{12}$ ions/cm^2 shows a value for $j_c(\Phi t)$ near to the theoretical limit, $j_{c,\max}$, due to columnar tracks. Curved flux lines are pinned nearly on their whole length by many pinning sites due to the resulting high density of defects. So, the effectiveness of extended spherical pinning sites in thin films is as large as that of the columnar tracks due to lead irradiation. As the relative enhancement of j_c found on nickel-irradiated DyBCO single crystals using the same fluences is similar to those obtained in thin films, the irradiation with Ni ions at large fluences produces defects which are not comparable in size and shape to the columnar tracks created by lead ions. The effectiveness of the pinning centers produced by Ni irradiation is only due to their large density.

Such a large value of $j_c(\Phi t)$ is also found at sample Y4, irradiated at a fluence $\Phi t = 6.0 \times 10^{14}$ ions/cm^2 where the critical current density is enhanced to $j_c(\Phi t) = 7.2 \times 10^7$ ions/cm^2. In Ref. 12, the displacement per atom (dpa) due to irradiation was calculated as $n = 4.8 \times 10^{-18}$ cm$^2 \cdot \Phi$. To obtain an enhancement of j_c, not only the direct displacement of atoms contributes to enhancement of the volume pinning forces, mainly the formation of defect cascades which are oriented perpendicular to the paths of the projectiles and consist of displaced atoms, is responsible for the enhancement of j_c. If the irradiation fluence is large enough, the so-produced defects show a similar pinning effect as the defects created by irradiation with nickel ions. For the irradiation with 25-MeV oxygen ions we have chosen samples made by Roas *et al.*[16] This allows a comparison of our results to the previous work concerning oxygen irradiation by Roas *et al.*[12] The enhancement of the critical current densities in our observations coincides well with the results of Roas *et al.* In the following, we will discuss various sources of pinning in the high-T_c superconductors and a possible simulation of these defects by heavy-ion irradiation. It is widely accepted in the literature that intrinsic pinning is present in the high-T_c materials if the magnetic field is applied perpendicular to the c axis.[33–35] Another source of pinning may be due to pinning at surfaces, which at present is only suggested by a few authors.[35] Crystal defects which are important for the pinning in high-T_c superconductors are point defects,[36] chemical impurity phases,[37–39] stacking faults,[40] screw dislocations,[14,15,41] and twin boundaries.[42,43] We will focus attention in the following to the crystal defects which can be produced by heavy-ion irradiation. The heavy-ion irradiation offers a method to induce defects of the same geometry as the background pinning sources up to even larger defect densities without the technological problems which will arise in processing samples with well-defined varying defect densities.

In the literature, screw dislocations are described as sources of the high-j_c values found in thin films.[14,15,41] In STM analysis,[44–46] the maximum defect density of these dislocations was measured to be 1.5×10^9 dislocations/cm^2. The dislocation core was assumed to be aligned parallel to the c axis of the thin film and is considered to act as the pinning center. The columnar tracks induced by lead irradiation have a geometry similar to these dislocation cores, so a direct comparison of both kinds of defects becomes possible. Our investigations on heavy-ion irradiation-induced defects reveal that a given enhancement of the critical current density, $j_{c,\mathrm{lim}}$, corresponds to each irradiation fluence. To reach the theoretical value of $j_{c,\max}$, an irradiation fluence of $\Phi t = 30.0 \times 10^{10}$ ions/cm^2 is required which is a factor of 200 larger than the maximum density of screw dislocations measured so far. If we calculate a dose-equivalent field, B_{screw}, but using the maximum density of screw dislocations, we obtain $B_{\mathrm{screw}} = 30$ mT. This field will be reached at small external magnetic fields of $\mu_0 H_{\mathrm{ext}} \approx 4$ mT due to the large demagnetizing factors of the thin films (see, also, the flux-density profiles of Fig. 2). The curvature of the flux lines is to be regarded. As shown in the discussion above, the influence of the curvature of the flux lines is stronger at low-defect densities than at large defect densities.

STM measurements[47] have shown that screw dislocations are also present in YBCO single crystals with approximately the same density as in thin films of YBCO. So, the background pinning in thin films and single crystals due to screw dislocations is approximately equal. This also shows that a comparison of the effects of heavy-ion irradiation in single crystals and thin films is possible.

The chemical impurity phases such as Y_2O_3 and Y_2BaCuO_5 have platelet or needlelike shapes as found in HRTEM observations[37–39,48] in thin films of YBCO. The density of these defects is approximately 10^{16} cm^{-3} and the diameters of these precipitations are in the range from 50 to 100 nm.[37] The irradiation of superconductors with ions such as nickel or oxygen allows a simulation of the pinning effect of these precipitations, if a large irradiation fluence is used. The so-induced defects act as effective pinning centers as can be seen from the domain

patterns obtained on samples Y1–Y7.

These results suggest that such chemical impurity phases play a major role in the background pinning. The large number of such defects found in thin films also implies that such samples have a granular structure. So, also, pinning at grain boundaries as in the case of Nb_3Sn (Refs. 49–51) might contribute to the background pinning.

VI. CONCLUSIONS

We have shown that the HRF technique is a very useful tool with which to investigate the effects of irradiation-induced defects also in YBCO thin films. Our method also provides the possibility to study simultaneously the flux penetration in irradiated and unirradiated areas of a single partly irradiated sample. In a well-defined sample geometry it is possible to reconstruct the domain patterns which would be obtained in a nonirradiated or fully irradiated sample.

We have shown that the most effective pinning centers are created by the formation of columnar tracks due to lead irradiation. The data obtained at the largest fluence of $\Phi t = 30.0 \times 10^{10}$ ions/cm^2, reach the theoretical limit, $j_{c,\max}$, for the enhancement of j_c due to the creation of columnar tracks. Our investigations suggest the existence of an experimental limit, $j_{c,\lim}$, which is not dependent on the target material corresponding to each irradiation fluence and to each projectile. This limit is smaller than $j_{c,\max}$ due to a local variation of the defect density thus leading to pinning-free paths for the flux lines.

At high-irradiation fluences, nickel and oxygen irradiation also produce very effective pinning sites leading to j_c data which are comparable to $j_{c,\max}$. The effectiveness of these pinning centers is caused only by their large density. It is shown that the heavy-ion irradiation provides a method to simulate pinning centers which are present in the background pinning without the technological problems which will arise in the preparation of samples with varying defect structures. A comparison of the pinning behavior of lead-irradiation-induced columnar tracks to that of screw dislocations clearly indicates that the density of screw dislocations is far too low to be responsible for the large j_c values found in thin films. Our results suggest that chemical impurity phases, whose pinning behavior can be simulated by irradiation with nickel or oxygen ions, play a major role in the background pinning.

ACKNOWLEDGMENTS

The authors want to thank M. Lippert, W. Dorsch, and G. Kreiselmeyer (University of Erlangen), B. Roas and L. Schultz (Siemens Laboratories, Erlangen), E.H. Brandt, U. Eßmann, B. Ludescher, P. Keppler, and E. Lutkat (MPI Stuttgart) for assistance and helpful discussions. The authors are indebted to S. Klaumünzer (HMI Berlin) and to S. Bouffard (GANIL, Caen, France). Financial support by the Bundesministerium für Forschung und Technologie and by the Bayerische Forschungsstiftung (FORSUPRA) is gratefully acknowledged.

[1] L. Civale, A.D. Marwick, T.K. Worthington, M.A. Kirk, J.R. Thompson, L. Krusin-Elbaum, Y. Sun, J.R. Clem, and F. Holtzberg, Phys. Rev. Lett. **67**, 648 (1991).

[2] W. Gerhäuser, G. Ries, H.-W. Neumüller, W. Schmidt, O. Eibl, G. Saemann-Ischenko, and S. Klaumünzer, Phys. Rev. Lett. **68**, 879 (1992).

[3] V. Hardy, J. Provost, D. Groult, M. Hervieu, B. Raveau, S. Durcok, E. Pollert, J.C. Frison, J.P. Chaminade, and M. Pouchard, Physica (Amsterdam) C **191**, 85 (1992).

[4] M. Leghissa, Th. Schuster, W. Gerhäuser, S. Klaumünzer, M.R. Koblischka, H. Kronmüller, H. Kuhn, H.-W. Neumüller, and G. Saemann-Ischenko, Europhys. Lett. **19**, 323 (1992).

[5] J.R. Thompson, Y.R. Sun, H.R. Kerchner, D.K. Christen, B.C. Sales, B.C. Chakoumakos, A.D. Marwick, L. Civale, and J.O. Thomson, Appl. Phys. Lett. **60**, 2306 (1992).

[6] Th. Schuster, M.R. Koblischka, H. Kuhn, H. Kronmüller, M. Leghissa, W. Gerhäuser, G. Saemann-Ischenko, H.-W. Neumüller, and S. Klaumünzer, Phys. Rev. B **46**, 8496 (1992).

[7] Th. Schuster, M. Leghissa, M.R. Koblischka, H. Kuhn, M. Kraus, H. Kronmüller, and G. Saemann-Ischenko, Physica C (to be published).

[8] D. Bourgault, S. Bouffard, T. Toulemonde, D. Groult, J. Provost, F. Studer, N. Nguyen, and B. Raveau, Phys. Rev. B **39**, 6549 (1989).

[9] A. Gupta, P. Esquinazi, H.F. Braun, H.-W. Neumüller, G. Ries, W. Schmidt, and W. Gerhäuser, Physica (Amsterdam) C **170**, 95 (1990).

[10] V. Hardy, D. Groult, J. Provost, M. Hervieu, B. Raveau, and S. Bouffard, Physica (Amsterdam) C **178**, 255 (1991).

[11] V. Hardy, D. Groult, J. Provost, and B. Raveau, Physica (Amsterdam) **190**, 289 (1992).

[12] B. Roas, B. Hensel, G. Saemann-Ischenko, and L. Schultz, Appl. Phys. Lett. **54**, 1051 (1989).

[13] B. Roas, B. Hensel, S. Henke, S. Klaumünzer, B. Kabius, H. Watanabe, G. Saemann-Ischenko, L. Schultz, and K. Urban, Europhys. Lett. **11**, 669 (1990); P. Schmitt, thesis, University of Erlangen (1992).

[14] J. Mannhart, D. Anselmetti, J.G. Bednorz, A. Catana, Ch. Gerber, K.A. Müller, and D.G. Schlom, Z. Phys. B **86**, 177 (1992).

[15] C. Gerber, D. Anselmetti, J.G. Bednorz, J. Mannhart, and D.G. Schlom, Nature (London) **350**, 279 (1991).

[16] B. Roas, G. Endres, and L. Schultz, Appl. Phys. Lett. **53**, 1557 (1988).

[17] Th. Schuster, M.R. Koblischka, H. Kuhn, M. Leghissa, M. Lippert, and H. Kronmüller, Physica (Amsterdam) C **196**, 373 (1992).

[18] K.-H. Greubel, E. Gmelin, N. Moser, Ch. Mensing, and L. Walz, Cryogenics **30** (Suppl.), 457 (1990).

[19] B. Ludescher, Th. Schuster, M.R. Koblischka, N. Moser, and H. Kronmüller, Laser Optoelektron. **23**, 54 (1991).

[20] Th. Schuster, M.R. Koblischka, N. Moser, B. Ludescher, and H. Kronmüller, Cryogenics **31**, 811 (1991).

[21] M.R. Koblischka, N. Moser, B. Gegenheimer, and H. Kronmüller, Physica (Amsterdam) C **166**, 36 (1990).

[22] A. Forkl, H.-U. Habermeier, B. Leibold, T. Dragon, and H. Kronmüller, Physica (Amsterdam) C **180**, 155 (1991).

[23] D. Glatzer, A. Forkl, H. Theuss, H.U. Habermeier, and H.

Kronmüller, Phys. Status Solidi B **170**, 549 (1992).
[24]H. Theuss, A. Forkl, and H. Kronmüller, Physica (Amsterdam) C **190**, 345 (1992).
[25]D.J. Frankel, J. Appl. Phys. **50**, 5402 (1979).
[26]M. Däumling and D.C. Larbalestier, Phys. Rev. B **40**, 9350 (1989).
[27]L.W. Conner and A.P. Malozemoff, Phys. Rev. B **43**, 402 (1991).
[28]Th. Schuster, M.R. Koblischka, B. Ludescher, and H. Kronmüller, Physica (Amsterdam) **C 179**, 269 (1991).
[29]Th. Schuster, M.R. Koblischka, B. Ludescher, and H. Kronmüller, J. Appl. Phys. **72**, 1478 (1992).
[30]E.H. Brandt, Europhys. Lett. **18**, 635 (1992); Phys. Rev. Lett. **69**, 1105 (1992).
[31]H. Watanabe, B. Kabius, K. Urban, B. Roas, S. Klaumünzer, and G. Saemann-Ischenko, Physica (Amsterdam) C **179**, 75 (1991).
[32]E.H. Brandt, Z. Phys. B **80**, 167 (1990); Physica (Amsterdam) C **195**, 1.
[33]M. Tachiki and S. Takahashi, Solid State Commun. **70**, 291 (1989).
[34]L. Schimmele, H. Kronmüller, and H. Teichler, Phys. Status Solidi B **147**, 361 (1988).
[35]B. Roas, L. Schultz, and G. Saemann-Ischenko, Phys. Rev. Lett. **64**, 479 (1990).
[36]T.L. Hylton and M.R. Beasley, Phys. Rev. B **41**, 11 669 (1990).
[37]A. Catana, F.R. Broom, J.G. Bednorz, J. Mannhart, and D.G. Schlom, Appl. Phys. Lett. **60**, 1016 (1992).
[38]K. Watanabe, T. Matsushita, N. Kobayashi, H. Kawabe, E. Aoyagi, K. Hiraga, H. Yamane, H. Kurosawa, T. Hirai, and Y. Muto, Appl. Phys. Lett. **56**, 1490 (1990).
[39]M. Murakami, S. Gotoh, N. Koshizuka, S. Tanaka, T. Matsushita, S. Kambe, and K. Kitazawa, Cryogenics **30**, 390 (1990).
[40]M. Murakami, S. Gotoh, H. Fujimoto, K. Yamaguchi, N. Koshizuka, and S. Tanaka, Supercond. Sci. Technol. **4**, 543 (1991); P. J. Kung, M. P. Maley, M. E. McHenry, J. O. Willis, J. Y. Coulter, M. Murakami, and S. Tanaka, Phys. Rev. B **46**, 6427 (1992).
[41]H. Douwes, P.H. Kes, Ch. Gerber, and J. Mannhart (unpublished).
[42]P.H. Kes, A. Pruynboom, J. van den Berg, and J.A. Mydosh, Cryogenics **29**, 228 (1989).
[43]D. Shi, M.S. Boley, J.G. Chen, M. Tang, U. Welp, W.K. Kwok, and B. Malecki, Supercond. Sci. Tech. **3**, 222 (1990).
[44]H.P. Lang, T. Frey, and H.-J. Günterodt, Europhys. Lett. **15**, 667 (1991).
[45]D.G. Schlom, D. Anselmetti, J.G. Bednorz, R.F. Broom, A. Catana, T. Frey, Ch. Gerber, H.-J. Güntherodt, H.P. Lang, and J. Mannhart, Z. Phys. B **86**, 163 (1992).
[46]M. Hawley, I.D. Raistrick, J.G. Beery, and R.J. Houlton, Science **251**, 1587 (1991); J. Burger, P. Bauer, M. Veith, and G. Saemann-Ischenko, Ultramicroscopy **42-44**, 721 (1992).
[47]A.V. Narlikar, P.K. Dutta, S.B. Samanta, O.N. Srivastava, P. Ramasamy, S.C. Sabarwal, M.K. Gupta, and B.D. Padalia, Appl. Phys. Lett. **60**, 1896 (1992).
[48]O. Eibl and B. Roas, J. Mater. Res. **5**, 2620 (1990).
[49]G. Zerweck, J. Low Temp. Phys. **42**, 1 (1981).
[50]R. Potratz, W. Klein, H.U. Habermeier, and H. Kronmüller, Phys. Status Solidi A **60**, 417 (1980).
[51]N. Moser, M.R. Koblischka, and H. Kronmüller, J. Less-Common Met. **164-165**, 1308 (1990).

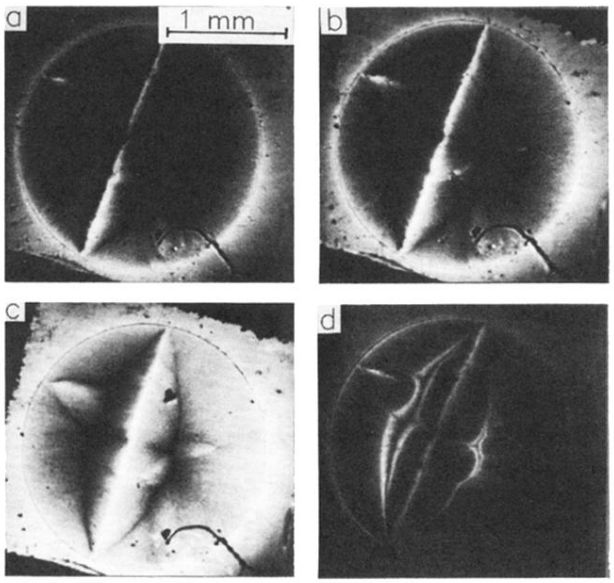

FIG. 1. Domain patterns observed on sample Y4 (oxygen irradiation, $\Phi t = 6.0 \times 10^{14}$ ions/cm^2). The Shubnikov phase is imaged as bright domains, the Meissner phase remains dark. On the substrate, which is also covered with the magneto-optical active layer, the local flux density, B_z, outside of the sample is detected. Only the left half of the sample was exposed to the irradiation. (a) $\mu_0 H_{\text{ext}} = 27$ mT. Due to the large demagnetizing factor of the thin film, the flux penetrates immediately along the border between the irradiated and the nonirradiated parts of the sample. (b) $\mu_0 H_{\text{ext}} = 109$ mT. (c) $\mu_0 H_{\text{ext}} = 273$ mT. The full penetration field, $\mu_0 H^*$, is nearly reached in the nonirradiated area. (d) The corresponding remanent state ($\mu_0 H_{\text{ext}} = 0$ mT) to (c). At the sample edges, flux lines of negative sign are clearly visible.

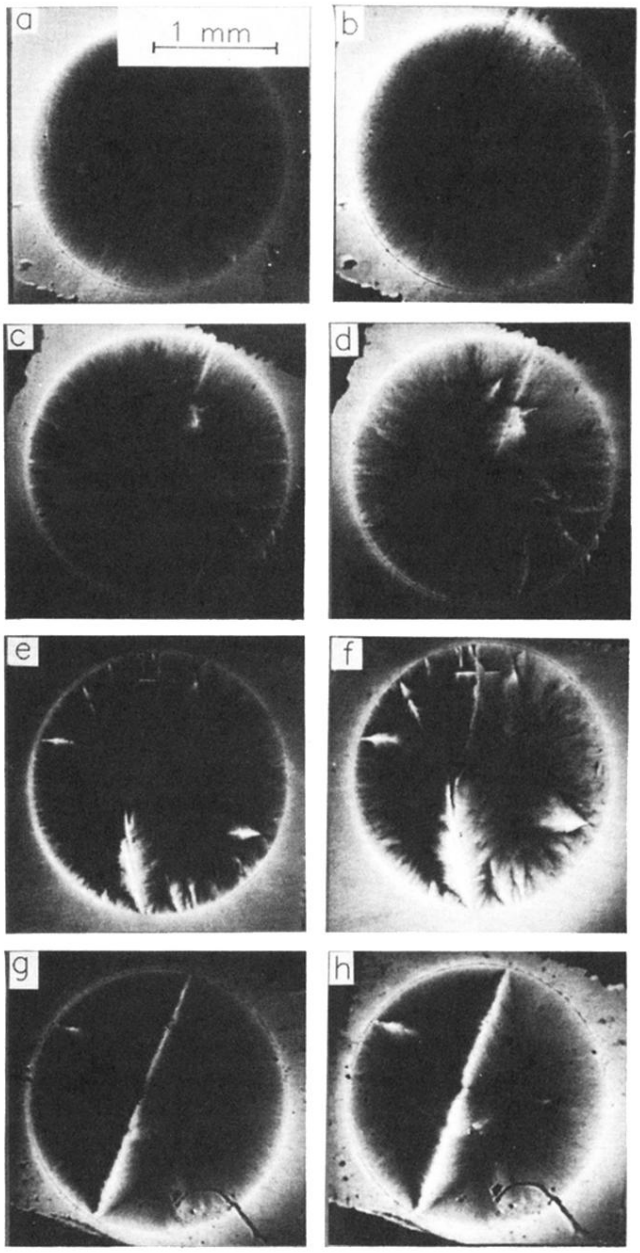

FIG. 5. Fluence dependence of the domain patterns obtained from oxygen irradiated samples. All thin films (laser-ablated films prepared at Siemens Laboratories, Erlangen) have the same thickness of 300 nm. (a) Sample Y1, irradiated at $\Phi t = 1.0 \times 10^{14}$ ions/cm^2. The external magnetic field is $\mu_0 H_{\text{ext}} = 27$ mT. (b) $\mu_0 H_{\text{ext}} = 109$ mT. No visible difference between the two areas is found in this sample. (c) Sample Y2, irradiated at $\Phi t = 2.0 \times 10^{14}$ ions/cm^2. The external magnetic field is $\mu_0 H_{\text{ext}} = 27$ mT. (d) $\mu_0 H_{\text{ext}} = 109$ mT. (e) Sample Y3, irradiated at $\Phi t = 4.0 \times 10^{14}$ ions/cm^2. The external magnetic field is $\mu_0 H_{\text{ext}} = 27$ mT. (f) $\mu_0 H_{\text{ext}} = 109$ mT. (g) Sample Y4, irradiated at $\Phi t = 6.0 \times 10^{14}$ ions/cm^2. The external magnetic field is $\mu_0 H_{\text{ext}} = 27$ mT. (h) $\mu_0 H_{\text{ext}} = 109$ mT.

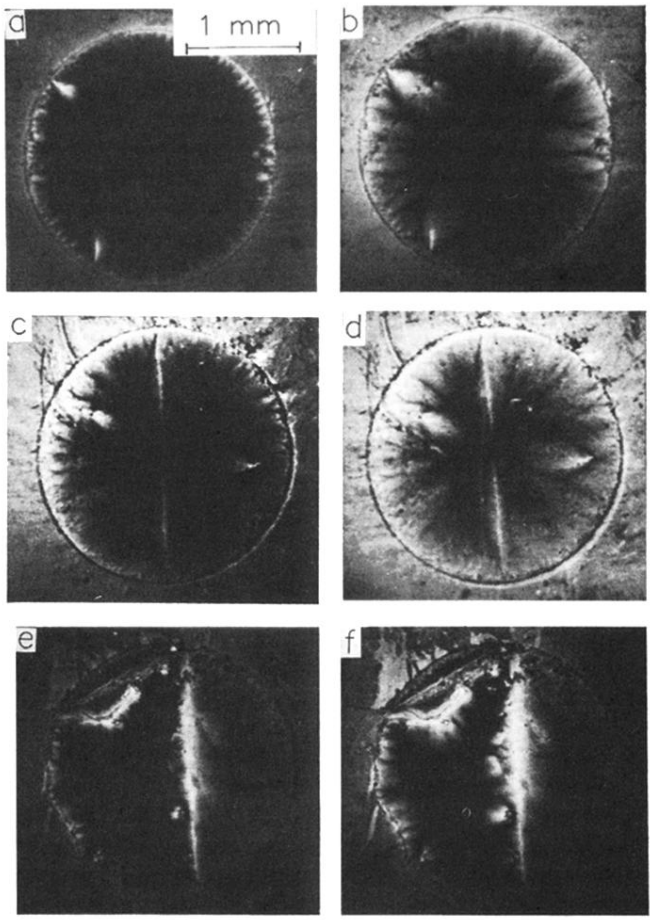

FIG. 6. Fluence dependence of the domain patterns after 230-MeV Nickel irradiation. The YBCO thin films were prepared at the University of Erlangen using a sputter technique; the film thickness is 450 nm. (a) Sample Y5, $\Phi t = 2.0 \times 10^{11}$ ions/cm^2, $\mu_0 H_{\text{ext}} = 68$ mT. (b) $\mu_0 H_{\text{ext}} = 178$ mT. (c) Sample Y6, $\Phi t = 5.0 \times 10^{11}$ ions/cm^2, $\mu_0 H_{\text{ext}} = 68$ mT. (d) $\mu_0 H_{\text{ext}} = 178$ mT. (e) Sample Y7, $\Phi t = 1.0 \times 10^{12}$ ions/cm^2, $\mu_0 H_{\text{ext}} = 68$ mT. (f) $\mu_0 H_{\text{ext}} = 178$ mT. This sample is the only one of this series showing a visible irradiation effect.

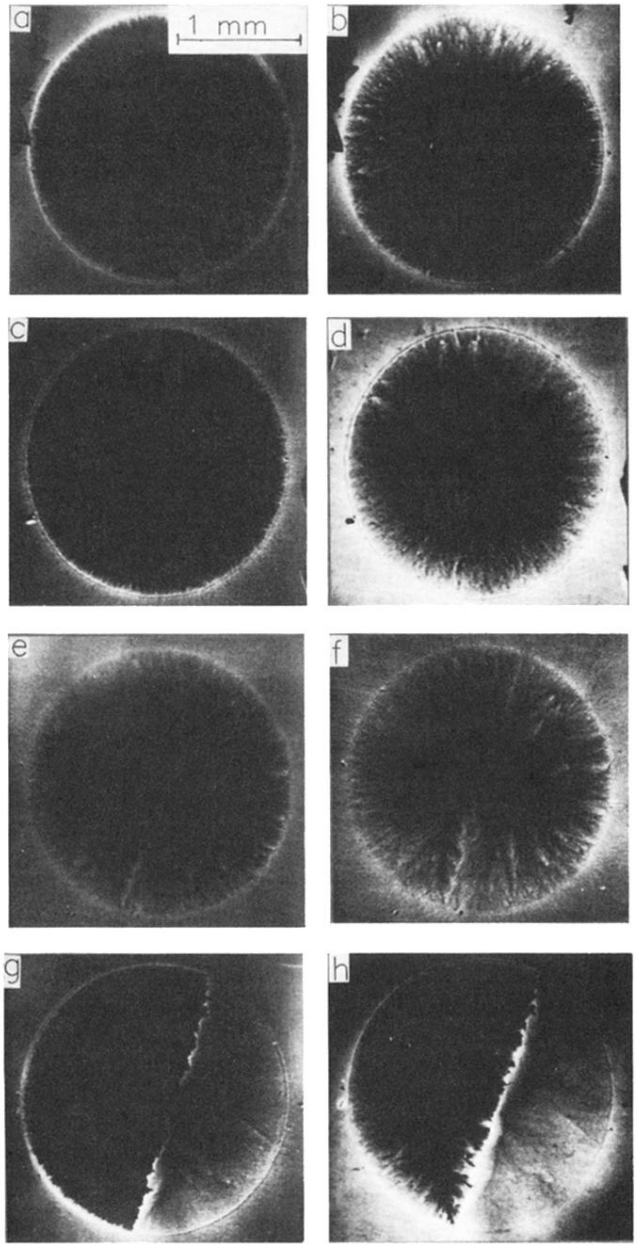

FIG. 7. Fluence dependence of the domain patterns after lead irradiation (1-GeV lead ions). These experiments are also performed on sputtered YBCO thin films with a thickness of 450 nm. (a) Sample Y8, irradiated at $\Phi t = 7.0 \times 10^{10}$ ions/cm^2, $\mu_0 H_{\text{ext}} = 27$ mT. (b) $\mu_0 H_{\text{ext}} = 109$ mT. The domain pattern shows no visible difference between irradiated and unirradiated areas. (c) Sample Y9 ($\Phi t = 9.0 \times 10^{10}$ ions/cm^2), $\mu_0 H_{\text{ext}} = 27$ mT. (d) $\mu_0 H_{\text{ext}} = 109$ mT. Also this sample shows a radial symmetric flux penetration. (e) Sample Y10 ($\Phi t = 10.0 \times 10^{10}$ ions/cm^2), $\mu_0 H_{\text{ext}} = 14$ mT. (f) $\mu_0 H_{\text{ext}} = 35$ mT. (g) Sample Y11, irradiated at $\Phi t = 30.0 \times 10^{10}$ ions/cm^2, $\mu_0 H_{\text{ext}} = 27$ mT. This sample is the only one in this series showing a large enhancement of j_c. (h) $\mu_0 H_{\text{ext}} = 109$ mT.